

# 6D Movable Antenna Enhanced Cell-free MIMO: Two-timescale Decentralized Beamforming and Antenna Movement Optimization

Yichi Zhang, Yuchen Zhang, *Member, IEEE*, Wenyan Ma, *Graduate Student Member, IEEE*, Lipeng Zhu, *Member, IEEE*, Jianquan Wang, *Member, IEEE*, Wanbin Tang, *Member, IEEE*, and Rui Zhang, *Fellow, IEEE*

**Abstract**—This paper investigates a six-dimensional movable antenna (6DMA)-aided cell-free multi-user multiple-input multiple-output (MIMO) communication system. In this system, each distributed access point (AP) can flexibly adjust its array orientation and antenna positions to adapt to spatial channel variations and enhance communication performance. However, frequent antenna movements and centralized beamforming based on global instantaneous channel state information (CSI) sharing among APs entail extremely high signal processing delay and system overhead, which is difficult to be practically implemented in high-mobility scenarios with short channel coherence time. To address these practical implementation challenges and improve scalability, a two-timescale decentralized optimization framework is proposed in this paper to jointly design the beamformer, antenna positions, and array orientations. In the short timescale, each AP updates its receive beamformer based on local instantaneous CSI and global statistical CSI. In the long timescale, the central processing unit optimizes the antenna positions and array orientations at all APs based on global statistical CSI to maximize the ergodic sum rate of all users. The resulting optimization problem is non-convex and involves highly coupled variables, thus posing significant challenges for obtaining efficient solutions. To address this problem, a constrained stochastic successive convex approximation algorithm is developed. Numerical results demonstrate that the proposed 6DMA-aided cell-free system with decentralized beamforming significantly outperforms other antenna movement schemes with less flexibility and even achieves a performance comparable to that of the centralized beamforming benchmark.

**Index Terms**—Six-dimensional movable antenna (6DMA), cell-free MIMO, decentralized optimization, statistical CSI.

Yichi Zhang and Wanbin Tang are with the National Key Laboratory of Wireless Communications, University of Electronic Science and Technology of China, Chengdu 611731, China (e-mail: yczhang@std.uestc.edu.cn, wb.tang@uestc.edu.cn).

Yuchen Zhang is with the Electrical and Computer Engineering Program, Division of Computer, Electrical and Mathematical Sciences and Engineering (CEMSE), King Abdullah University of Science and Technology (KAUST), Thuwal, 23955-6900, Kingdom of Saudi Arabia (e-mail: yuchen.zhang@kaust.edu.sa).

Lipeng Zhu is with the School of Interdisciplinary Science, Beijing Institute of Technology, Beijing 100081, China (e-mail: lipzhu@outlook.com).

Wenyan Ma, and Rui Zhang are with the Department of Electrical and Computer Engineering, National University of Singapore, Singapore 117583 (e-mail: wenyan@u.nus.edu; elezhang@nus.edu.sg).

Jianquan Wang is with the National Key Laboratory of Wireless Communications, University of Electronic Science and Technology of China, Chengdu 611731, China, and also with the Kash Institute of Electronics and Information Industry, Kash 844000, China (e-mail: jqwang@uestc.edu.cn).

## I. INTRODUCTION

With the rapid evolution of wireless communications, the explosive growth of user and device connectivity has created an urgent demand for additional spectral resources. High-frequency bands such as millimeter-wave and terahertz have been regarded as key enablers for next-generation mobile communication networks. To compensate for severe path loss and improve signal coverage, it is necessary to employ large-scale antenna arrays and deploy access points (APs) more densely. However, in the traditional cell-centric networks, the resulting high signal dimensionality introduced by large-scale arrays at the central processing unit (CPU) leads to substantial hardware cost and signal processing complexity for centralized computing. Meanwhile, densely deployed APs in conventional cellular networks cause frequent handovers and strong inter-AP interference, thereby degrading the performance of cell-edge users.

To address these challenges, cell-free massive multi-input multi-output (MIMO) has been proposed, in which a large number of distributed APs collaboratively serve users without cell boundaries under the coordination of a CPU. To further reduce the processing burden at the CPU, cell-free systems can leverage local processing unit (LPU) of each AP to locally process its received signals. Specifically, several studies have explored low-complexity decentralized beamforming schemes under different levels of channel state information (CSI) exchange [1]–[6]. In [1], local minimum mean-square error (LMMSE)-based beamforming methods were proposed in scenarios with no/statistical/full CSI sharing. In [2], an optimal beamformer design rule that minimizes mean-square error (MSE) under arbitrary CSI-sharing conditions was further developed. Building upon these LMMSE/MSE-based design strategies, the authors in [3]–[8] investigated decentralized architectures under specific scenarios, such as strong line of sight (LoS) channels, satellite communications, uplink power minimization, CSI sharing among APs based on a ring topology, and different levels of CSI sharing under channel uncertainty. However, in cell-free systems, the limited number of antennas at each AP makes it difficult to effectively mitigate inter-user interference. Moreover, most existing studies rely on fixed-position antennas (FPAs), which cannot fully exploit the spatial degrees of freedom (DoFs) in wireless systems.

To address the limitations of FPAs, movable antenna (MA), also known as fluid antenna system (FAS), has been proposed to improve wireless communication performance by flexibly adjusting antenna positions based on either instantaneous CSI or statistical CSI [9]–[12]. In [11], the authors first introduced the field-response-based channel model to analytically evaluate the performance gain of MA-aided single-input single-output (SISO) systems. Building on this model, subsequent works [12]–[19] applied the MA technique to various scenarios under instantaneous CSI, where real-time antenna movement was leveraged to characterize the performance limits of various systems, including MIMO, multi-user, satellite, unmanned aerial vehicle (UAV), integrated sensing and communication (ISAC), and hybrid beamforming-aided communications systems. To alleviate the latency and power consumption induced by real-time antenna movement based on instantaneous CSI, discrete antenna movement strategy [20], antenna movement trajectory optimization [21], and the upper bound on energy efficiency [22] were investigated to minimize movement delay or improve system energy efficiency. Furthermore, to avoid frequent antenna repositioning in high-mobility environments with relatively short channel coherence time, the authors in [23], [24] optimized antenna positions based on statistical CSI to maximize MIMO capacity. In addition, two-timescale designs for beamforming and antenna position optimization were proposed in [25], [26] to improve the ergodic sum rate under both conventional Rician fading and statistical field-response-based channel models. Overall, these studies demonstrated that MA-aided communication systems can achieve significant performance improvements under both instantaneous CSI and statistical CSI owing to their flexible spatial DoFs.

More recently, six-dimensional movable antenna (6DMA) has been proposed to further improve communication performance by jointly adjusting antenna positions and orientations, thereby fully exploiting spatial DoFs for channel reconfiguration and interference suppression [27]–[33]. In [27], the authors initially investigated 6DMA-aided multi-user communications and optimized the positions and orientations of 6DMA sub-arrays under LoS channels according to the user distribution. Numerical results demonstrated that 6DMA can provide substantial performance gains compared with the FPA baseline. Subsequently, [28]–[33] extended the 6DMA to various scenarios, including discrete antenna position/orientation optimization, hybrid beamforming, UAV communications, intelligent reflecting surfaces (IRS)-aided passive beamforming, and near-field communications. Moreover, the authors in [9], [34]–[36] introduced specific implementation architectures and practical considerations for 6DMA, such as channel estimation accuracy, CSI acquisition timeliness, and hardware constraints. It is worth noting that most existing studies on 6DMA-aided wireless networks rely on statistical CSI or user distribution to enable long-timescale antenna movement, aiming to achieve low-latency and cost-effective communication performance.

In particular, to enhance the communication performance in large-scale MIMO networks, prior works [37]–[39] have

integrated 6DMA into cell-free systems. The study in [39] adopted centralized beamforming and optimized antenna positions and orientations based on instantaneous CSI to support massive access and interference mitigation, whereas [37], [38] employed decentralized beamforming to reduce signal processing complexity. However, [37] considered an LMMSE-based beamformer design with no/full CSI sharing among APs, which represent two extreme cases and do not capture the potential gains under practical CSI sharing conditions. In addition, only LoS channels were considered for antenna movement optimization, which may result in significant performance degradation under practical multi-path fading channels that vary too fast for the antennas to adapt to due to limited antenna moving speeds. In contrast, the authors in [38] improved the decentralized beamforming design by introducing statistical CSI sharing among APs but relying on real-time array reconfiguration, making it difficult to cope with the latency induced by frequent array rotations. Moreover, this work focused solely on array rotation, which restricts the available design DoFs for reducing inter-user channel correlation, particularly in dense-user scenarios. Such limitation motivates a new design framework proposed in this paper for 6DMA-aided cell-free systems.

In this work, we study a 6DMA-aided uplink cell-free multi-user MIMO (MU-MIMO) communication system, where antennas at each AP can move independently on an array panel, while the array panel can also rotate together with its antennas as a single unit. The main contributions are as follows.

- To balance the antenna movement overhead and MIMO network performance, we develop a two-timescale decentralized optimization framework that maximizes the ergodic sum rate of all users. In the short timescale, each AP designs its LMMSE receive beamformer using its local instantaneous CSI together with the statistical CSI shared among the APs. In the long timescale, the CPU optimizes antenna positions and array orientations based on global statistical CSI.
- To efficiently solve the non-convex long timescale antenna position and array orientation optimization problem, we reformulate a relaxed problem that treats the long-timescale parameters as independent optimization variables and propose a constrained stochastic successive convex approximation (CSSCA) algorithm to solve the coupled variables in parallel.
- Simulation results show the performance gain of 6DMA under both concentrated and uniformly distributed user scenarios. It is demonstrated that the proposed 6DMA-aided cell-free system outperforms the conventional FPA and other antenna movement schemes with less flexibility under different user distribution scenarios. Moreover, under specific conditions such as weaker inter-user channel correlations as well as sufficiently large movable regions or rotatable ranges, the proposed scheme can even surpass the performance of the centralized minimum mean-square error (MMSE) benchmark with FPAs that assumes full

CSI sharing among all APs. Moreover, the results indicate that the performance improvement becomes more pronounced under sparse user distributions, owing to the reduced channel correlation among users.

The rest of this paper is organized as follows. Section II describes the system model and formulates the problem. Section III derives the optimal receive beamformer design rule over short timescale and then to solve the formulated long-timescale problem by the CSSCA algorithm. Section IV presents numerical results and pertinent discussions. Finally, Section V concludes the paper.

*Notations:* Vectors and matrices are denoted in boldface with lower case and upper case, respectively. We use  $(\cdot)^T$ ,  $(\cdot)^*$ , and  $(\cdot)^H$  to denote the transpose, conjugate, and conjugate transpose, respectively. The notations  $\mathbb{C}^{M \times N}$  and  $\mathbb{R}^{M \times N}$  denote the set of  $M \times N$  dimensional complex and real matrices, respectively. The notations  $\mathbb{E}$  and  $\mathbb{V}$  are the mathematical expectation and variance operators, respectively. We use  $\mathbf{I}_N$  to denote the  $N$ -dimensional identity matrix,  $\mathbf{e}_n \in \mathbb{R}^{N \times 1}$  to denote the  $N$ -dimensional column vector with the  $n$ -th element being 1 and all others being 0, and  $\mathbf{A} = \text{blkdiag}[\mathbf{A}_1, \mathbf{A}_2, \dots, \mathbf{A}_N]$  to denote a block diagonal matrix. The notation  $[f(n)]_{1 \leq n \leq N}$  denotes a vector with the  $n$ -th element being  $f(n)$ , where  $f(n)$  is a function w.r.t.  $n$ ,  $\|\mathbf{a}\|_2$  is the 2-norm of vector  $\mathbf{a}$ . We use  $\arccos(\cdot)$  to denote the arccosine function,  $|b|$  and  $\angle(b)$  are amplitude and phase of the complex number  $b$ , and  $\text{Re}\{b\}$  denotes the real part of  $b$ .

## II. SYSTEM MODEL

This section first presents the system model of the 6DMA-aided cell-free network. A field-response-based statistical channel model is then adopted to characterize the phase and amplitude variations of quasi-static propagation paths at APs, which are induced by antenna movement and array rotation [11], [23], [26]–[28], [37], [40], [41]. Finally, the optimization problem is formulated to maximize the ergodic sum rate of all users, subject to practical antenna movement constraints.

### A. 6DMA-aided Cell-free Architecture

As illustrated in Fig. 1, we consider a 6DMA-aided cell-free MU-MIMO uplink system, where  $M$  multi-antenna APs, each equipped with  $N$  antennas, serve  $K$  single-antenna users. A decentralized architecture is considered, where each AP independently processes its received signals with an LPU while exchanging signaling and payload data with the CPU via a dedicated fronthaul link. The array of each AP is capable of rotating around its geometric center. In addition, each antenna can move independently on the array plane driven by step motors. Due to practical implementation requirements, antenna movements and array rotations are restricted to a predefined range, and the inter-antenna spacing is no smaller than half a wavelength during antenna movement to avoid heavy mutual coupling.

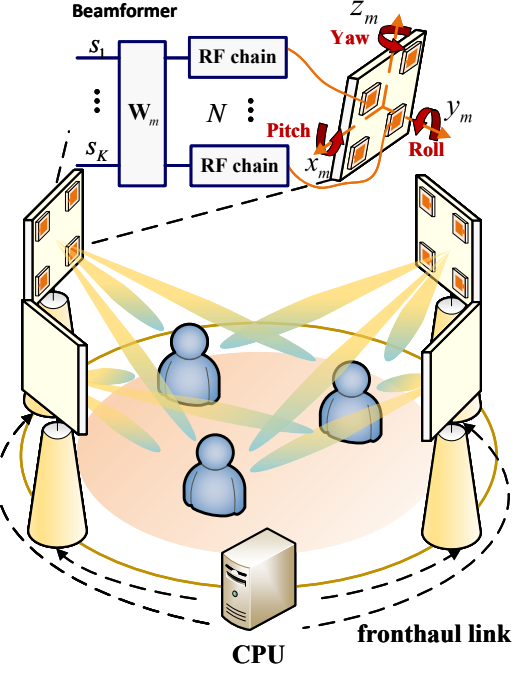


Fig. 1. Illustration of the 6DMA-aided cell-free MU-MIMO system.

For the array of the  $m$ -th AP, the red dotted line in Fig. 1 denotes its local Cartesian coordinate system (LCS)  $x_m$ - $y_m$ - $z_m$ . The origin of this LCS is fixed at the geometric center of the supporting plane, and its axes are aligned with the orientation of the array. The array orientation of the  $m$ -th AP is denoted by  $\mathbf{r}_m = [\alpha_m, \beta_m, \gamma_m]^T \in \mathcal{R}$ , where  $\mathcal{R}$  denotes the feasible rotation region. Specifically,  $\alpha_m$ ,  $\beta_m$ , and  $\gamma_m$  represent the pitch, roll, and yaw angles of the  $m$ -th AP's rotation around the  $x$ -axis,  $y$ -axis, and  $z$ -axis with respect to (w.r.t.) its initial orientation, respectively. The positions of all antennas within the  $m$ -th AP's LCS are collected as  $\mathbf{t}_m = [\mathbf{t}_{m,1}^T, \mathbf{t}_{m,2}^T, \dots, \mathbf{t}_{m,N}^T]^T \in \mathbb{R}^{3N \times 1}$ , where  $\mathbf{t}_{m,n} \in \mathcal{T}_{m,n}$  denotes the position of the  $n$ -th antenna at the  $m$ -th AP, with  $\mathcal{T}_{m,n}$  denoting the movable region of the  $n$ -th antenna.

### B. Statistical Channel Model

Since the predefined movable regions of antennas at all APs are much smaller than the propagation distance, the far-field assumption is adopted [11]–[16], [27]–[29]. Antenna movement and array rotation change the three-dimensional (3D) antenna positions, boresight of antenna radiation patterns, and angles of arrival (AoAs) of the received signals. Under the multi-path propagation environment, the azimuth and elevation angles of the  $l$ -th received path w.r.t. the LCS of the  $m$ -th AP, before and after array rotation, are denoted by  $(\phi_{l,m}, \theta_{l,m})$  and  $(\tilde{\phi}_{l,m}, \tilde{\theta}_{l,m})$ <sup>1</sup>, respectively.

1) *Array Response Vectors:* We proceed to express the effective transformation from  $(\phi, \theta)$  to  $(\tilde{\phi}, \tilde{\theta})$ . Letting

<sup>1</sup>For brevity, the subscripts associated with user indexes are omitted here, while the detailed channel model will be presented later.

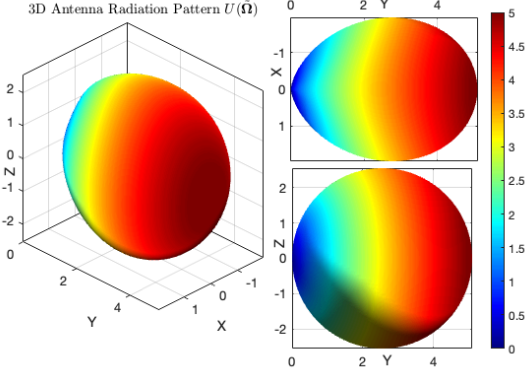


Fig. 2. Illustration of the cosine radiation pattern [43].

$\Omega_{l,m} \triangleq [\phi_{l,m}, \theta_{l,m}]$  with  $\phi_{l,m} \in [0, 2\pi)$  and  $\theta_{l,m} \in [0, \pi]$ , the normalized wave vector pointing to the wave direction  $(\phi_{l,m}, \theta_{l,m})$  is given by  $\rho_{l,m} \triangleq \rho(\Omega_{l,m}) = [\sin \theta_{l,m} \cos \phi_{l,m}, \sin \theta_{l,m} \sin \phi_{l,m}, \cos \theta_{l,m}]^T$ . We define  $\mathbf{R}_z$ ,  $\mathbf{R}_y$ , and  $\mathbf{R}_x$  as the LCS transformation induced only by rotating w.r.t.  $z$ -axis,  $y$ -axis, and  $x$ -axis, respectively. The rotation matrix  $\mathbf{R}$ , which describes the array orientation transformation of any AP, is expressed as

$$\begin{aligned} \mathbf{R}(\mathbf{r}) &= \mathbf{R}_z(\gamma) \mathbf{R}_y(\beta) \mathbf{R}_x(\alpha) \\ &= \begin{bmatrix} c_\gamma & -s_\gamma & 0 \\ s_\gamma & c_\gamma & 0 \\ 0 & 0 & 1 \end{bmatrix} \begin{bmatrix} c_\beta & 0 & s_\beta \\ 0 & 1 & 0 \\ -s_\beta & 0 & c_\beta \end{bmatrix} \begin{bmatrix} 1 & 0 & 0 \\ 0 & c_\alpha & -s_\alpha \\ 0 & s_\alpha & c_\alpha \end{bmatrix} \\ &= \begin{bmatrix} c_\beta c_\gamma & s_\alpha s_\beta c_\gamma - c_\alpha s_\gamma & c_\alpha s_\beta c_\gamma + s_\alpha s_\gamma \\ c_\beta s_\gamma & s_\alpha s_\beta s_\gamma + c_\alpha c_\gamma & c_\alpha s_\beta s_\gamma - s_\alpha c_\gamma \\ -s_\beta & s_\alpha c_\beta & c_\alpha c_\beta \end{bmatrix}, \end{aligned} \quad (1)$$

where  $c_\alpha = \cos \alpha$  and  $s_\alpha = \sin \alpha$  for concise. Letting  $\mathbf{R}_m \triangleq \mathbf{R}(\mathbf{r}_m)$ , based on the geometric transformation, the direction vector of the  $l$ -th path w.r.t. the LCS of the  $m$ -th AP after array rotation is given by  $\tilde{\rho}_{l,m} \triangleq \rho(\tilde{\Omega}_{l,m}) = \mathbf{R}_m^T \rho_{l,m}$  [42], thus leading to

$$\tilde{\phi}_{l,m} = \angle([1, j, 0] \mathbf{R}_m^T \rho_{l,m}), \quad (2a)$$

$$\tilde{\theta}_{l,m} = \arccos([0, 0, 1] \mathbf{R}_m^T \rho_{l,m}). \quad (2b)$$

The array response vector of the  $m$ -th AP for the  $l$ -th received path is then given by

$$\mathbf{a}(\mathbf{t}_m, \mathbf{r}_m, \Omega_{l,m}) = \left[ e^{j \frac{2\pi}{\lambda} \rho_{l,m}^T \mathbf{R}_m \mathbf{t}_m} \right]_{1 \leq n \leq N}^T, \quad (3)$$

where  $\lambda$  denotes the carrier wavelength.

2) *Directional Radiation Pattern*: The array rotation also results in the variation of the boresight of each antenna's radiation pattern. As shown in Fig. 2, for the commonly used cosine radiation pattern [43], the effective antenna gain for the  $l$ -th channel path at the  $m$ -th AP is expressed as

$$U(\tilde{\Omega}_{l,m}) = \begin{cases} \frac{16}{\pi} \sin^2 \tilde{\phi}_{l,m} \sin \tilde{\theta}_{l,m}, & \tilde{\phi}_{l,m} \in [0, \pi), \\ 0, & \text{otherwise.} \end{cases} \quad (4)$$

Here, the radiated power is normalized by  $\int_{\Omega} U(\phi, \theta) d\Omega = 4\pi$  with  $\Omega$  representing the unit sphere. We define  $A_E(\mathbf{r}_m, \Omega_{l,m}) \triangleq \sqrt{U(\tilde{\Omega}_{l,m})}$  as the pattern coefficient along the propagation direction  $(\phi_{l,m}, \theta_{l,m})$ .

To accurately evaluate the performance of 6DMA in cell-free MIMO systems, it is essential to employ realistic channel models that capture key propagation characteristics. Most existing studies on 6DMA or cell-free systems rely on deterministic channel models to assess performance limits [1], [12]–[14], [17], [29], [39]. However, deterministic modeling, which assumes that the CPU has complete knowledge of the CSI obtained through ray-tracing or other channel estimation approaches, is challenging in practical deployments, as it entails substantial overhead for precise channel estimation and frequent antenna movement based on perfect CSI. Moreover, centralized processing, in which all APs collaboratively decode received signals through full CSI sharing, requires extensive data and signal exchange between the APs and the CPU, further increasing the system burden. In high-mobility environments, the short channel coherence time is insufficient to support such intensive channel estimation, antenna movement, and AP coordination. Motivated by these practical constraints, and to improve the applicability of 6DMA in realistic communication scenarios, we adopt a statistical channel model following prior works [2]–[4], [11], [23], [26], [40], [41].

Specifically, the field-response based channel model is considered. In this model, it is assumed that the CPU acquires the quasi-static AoAs for each AP, while the small-scale fading coefficients vary rapidly due to environmental dynamics. The channel response for narrow-band system between the  $m$ -th AP and the  $k$ -th user is expressed as the sum of the responses of multiple channel paths:

$$\mathbf{h}_{k,m} = \sum_{l=1}^{L_{k,m}} \psi_{k,l,m} A_E(\mathbf{r}_m, \Omega_{k,l,m}) \mathbf{a}(\mathbf{t}_m, \mathbf{r}_m, \Omega_{k,l,m}), \quad (5)$$

where  $L_{k,m}$  is the total number of received paths from the  $k$ -th user.  $\psi_{k,l,m} \sim \mathcal{CN}(0, b_{k,l,m})$  denotes the fading coefficient of the  $l$ -th received paths between the  $k$ -th user and the  $m$ -th AP, representing the small-scale fading effects associated with local scattering at the user side [26], [40], [41], with  $\{b_{k,l,m}\}$  being the average power. In this decentralized architecture, each AP needs to access to both the local instantaneous CSI and the global statistical CSI. The local instantaneous CSI at the  $m$ -th AP is denoted as  $\hat{\mathbf{H}}_m = [\hat{\mathbf{h}}_{1,m}, \hat{\mathbf{h}}_{2,m}, \dots, \hat{\mathbf{h}}_{K,m}]$ , corresponding to specific estimated values of the fading coefficients  $\{\psi_{k,l,m}\}_{l=1}^{L_{k,m}}\}_{k=1}^K$ . In contrast, the global statistical CSI corresponds to the distribution of the random fading channel coefficients.

### C. Signal Model

By collecting the channel vectors of all APs in  $\mathbf{h}_k = [\mathbf{h}_{k,1}^T, \mathbf{h}_{k,2}^T, \dots, \mathbf{h}_{k,M}^T]^T$ , the decoded signal of the  $k$ -th user

at the CPU is given by

$$y_k = \sum_{m=1}^M y_{k,m} = \mathbf{w}_k^H \left( \sum_{j=1}^K \mathbf{h}_j s_j + \mathbf{n} \right), \quad (6)$$

where  $s_k \sim \mathcal{CN}(0, 1)$  is the transmit signal from the  $k$ -th user,  $y_{k,m}$  denotes the signal decoded by the  $m$ -th AP from the  $k$ -th user,  $\mathbf{w}_k = [\mathbf{w}_{k,1}^H, \mathbf{w}_{k,2}^H, \dots, \mathbf{w}_{k,M}^H]^H \in \mathbb{C}^{MN \times 1}$  and  $\mathbf{w}_{k,m}$  are the receive beamformers for user  $k$  at the CPU and the  $m$ -th AP, respectively.  $\mathbf{n} \sim \mathcal{CN}(\mathbf{0}, \sigma^2 \mathbf{I}_{MN})$  is the received Gaussian noise.

Based on the derived channel model in (5) and signal model in (6), the achievable rate for the  $k$ -th user is given by

$$R_k = \log_2 \left( 1 + \frac{|\mathbf{w}_k^H \mathbf{h}_k|^2}{\sum_{j \neq k} |\mathbf{w}_k^H \mathbf{h}_j|^2 + \sigma^2 \|\mathbf{w}_k\|_2^2} \right). \quad (7)$$

Several practical challenges arise when applying 6DMA to cell-free networks. First, frequent CSI exchange among distributed APs introduces considerable communication overhead, making centralized receive beamformer design based on full CSI difficult and thereby motivating decentralized optimization. Second, the relatively short channel coherence time makes it difficult to perform real-time antenna movement and forward the updates to all APs. Frequent antenna adjustments may also lead to excessive processing latency and power consumption. Third, due to channel variations induced by antenna movement, the receive beamformer is coupled with antenna positions and array orientations, making joint optimization of the beamformer, antenna position, and array orientation highly challenging. To address these challenges, we propose a two-timescale design framework. In the short timescale, the receive beamformers at the  $m$ -th AP are determined at its LPU in closed form based on local instantaneous CSI. In the long timescale, antenna movement at each AP is performed using slow-varying statistical CSI, and the optimized antenna positions and array orientations are forwarded to all APs.

Denote  $\mathbf{t} = [\mathbf{t}_1^T, \mathbf{t}_2^T, \dots, \mathbf{t}_M^T]^T$ ,  $\mathbf{r} = [\mathbf{r}_1^T, \mathbf{r}_2^T, \dots, \mathbf{r}_M^T]^T$ , and  $\mathbf{W} = [\mathbf{w}_1, \mathbf{w}_2, \dots, \mathbf{w}_K]$  for notation simplicity. To maximize the ergodic sum rate of all users, the two-timescale optimization problem that jointly designs the receive beamformer  $\mathbf{W}$ , the array orientations  $\mathbf{r}$ , and the antenna positions  $\mathbf{t}$  of all APs is given by

$$\max_{\mathbf{t}, \mathbf{r}} \mathbb{E}_{\mathbf{H}} \left[ \max_{\mathbf{W}} \sum_{k=1}^K R_k \right] \quad (8a)$$

$$\text{s.t. } \mathbf{t}_{m,n} \in \mathcal{T}_{m,n}, \forall m, n, \quad (8b)$$

$$\mathbf{r}_m \in \mathcal{R}, \forall m, \quad (8c)$$

where  $\mathcal{R} = \{[\alpha, \beta, \gamma]^T | \alpha \in [\alpha^L, \alpha^U], \beta \in [\beta^L, \beta^U], \gamma \in [\gamma^L, \gamma^U]\}$  and  $\mathcal{T}_{m,n} = \{[x, y, z]^T | x \in [x_{m,n}^L, x_{m,n}^U], y \in [y_{m,n}^L, y_{m,n}^U], z \in [z_{m,n}^L, z_{m,n}^U]\}$  denote the predefined rotatable and movable ranges, respectively. The variables with superscripts L and U denote the lower and upper bounds on the corresponding variables, respectively. In the rest of the paper, the expectation operator  $\mathbb{E}[\cdot]$  is applied to the random channel

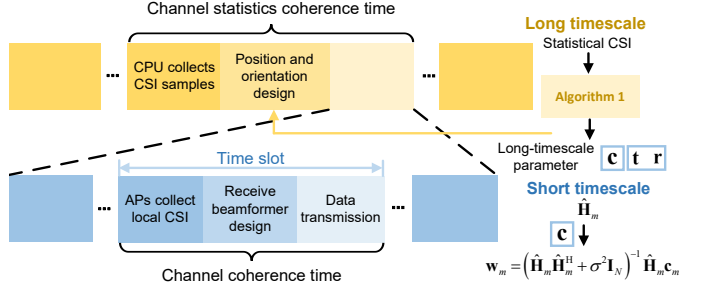


Fig. 3. Illustration of the two-timescale decentralized design framework, including the short-timescale workflow at each AP and the long-timescale workflow at the CPU.

matrix  $\mathbf{H}$  unless stated otherwise. It is important to note that optimizing the beamformer  $\mathbf{W}$  is a distributed process, where each AP optimizes its local receive beamformer based on the available CSI. This necessitates an update rule for the beamformer at each AP to enhance the overall sum rate. Furthermore, due to the expectation over  $\mathbf{H}$ , determining the optimal antenna positions and array orientations is challenging.

**Remark 1.** Due to the lack of instantaneous CSI from other APs, the receive beamformer at each AP should be updated in the short timescale by jointly exploiting the global statistical CSI and the local instantaneous CSI, as discussed in Section II-C. Consequently, in the formulation of the ergodic sum rate optimization problem (8), the receive beamformer,  $\mathbf{W}$ , should be regarded as a mapping from the available CSI to the receive beamforming matrix rather than as a fixed solution.

### III. TWO-TIMESCALE DECENTRALIZED DESIGN

In this section, we aim to solve problem (8). Specifically, a two-timescale design is proposed to balance practical feasibility and ergodic sum-rate performance. As illustrated in Fig. 3, the long-timescale parameter is treated as a constant within the short-timescale optimization, which are computed at the CPU and then distributed to all APs for local processing. To enable each AP to design its short-timescale receive beamformer in closed form based on local instantaneous CSI and global statistical CSI, the objective function is first approximated using the well-known use-and-then-forget (UatF) lower bound [44] for improved tractability. Subsequently, inspired by the fractional programming (FP) framework [45], the optimal receive beamformer is derived w.r.t. both statistical and local instantaneous CSI. In the long timescale, the CSSCA algorithm is employed to jointly optimize the antenna positions and array orientations in parallel to maximize the ergodic sum rate of all users.

#### A. Short-timescale Receive Beamformer Design

1) *FP-Based UatF Bound Optimization:* To efficiently derive a closed-form expression of the receive beamformer at each AP, we optimize the more tractable UatF lower bound

on the ergodic achievable rate for each AP, which is given by [44]

$$\sum_{k=1}^K \mathbb{E}[R_k] \geq \sum_{k=1}^K R_k^{\text{UatF}} = \sum_{k=1}^K \log(1 + \text{SINR}_k^{\text{UatF}}), \quad (9a)$$

$$\text{SINR}_k^{\text{UatF}} = \frac{|\mathbb{E}[\mathbf{w}_k^H \mathbf{h}_k]|^2}{\sum_{j \neq k} \mathbb{E}[|\mathbf{w}_k^H \mathbf{h}_j|^2] + \mathbb{V}[\mathbf{w}_k^H \mathbf{h}_k] + \sigma^2 \mathbb{E}[|\mathbf{w}_k|^2]}. \quad (9b)$$

Then, during the short timescale, given antenna positions  $\mathbf{t}$  and array orientations  $\mathbf{r}$ , the subproblem for optimizing receive beamformers can be written as

$$\max_{\mathbf{W}} \sum_{k=1}^K R_k^{\text{UatF}}. \quad (10)$$

According to the FP framework [45], the problem in (10) can be equivalently reformulated as

$$\min_{\mathbf{W}, \vartheta, \varpi} \sum_{k=1}^K (1 + \vartheta_k) \mathbb{E}[e_k(\varpi_k)] + \vartheta_k - \log(1 + \vartheta_k), \quad (11)$$

where  $\vartheta = \{\vartheta_k\}_{k=1}^K$  and  $\varpi = \{\varpi_k\}_{k=1}^K$  are both a set of the slack variables.  $\mathbb{E}[e_k(\varpi_k)]$  is given by

$$\begin{aligned} \mathbb{E}[e_k(\varpi_k)] &= |\varpi_k|^2 \left( \sum_{j \neq k} \mathbb{E}[|\mathbf{w}_k^H \mathbf{h}_j|^2] + \mathbb{V}[\mathbf{w}_k^H \mathbf{h}_k] \right. \\ &\quad \left. + \sigma^2 \mathbb{E}[|\mathbf{w}_k|^2] \right) - 2\text{Re}\{\varpi_k^* \mathbb{E}[\mathbf{w}_k^H \mathbf{h}_k]\} \\ &\stackrel{(a)}{=} \mathbb{E}\left[\|\varpi_k \mathbf{H}^H \mathbf{w}_k - \mathbf{e}_k\|_2^2 + \sigma^2 \|\varpi_k \mathbf{w}_k\|_2^2\right], \end{aligned} \quad (12)$$

where  $\mathbf{H} = [\mathbf{h}_1, \mathbf{h}_2, \dots, \mathbf{h}_K]$ . The equality (a) is derived using the identity  $\mathbb{V}[\mathbf{w}^H \mathbf{h}] = \mathbb{E}[|\mathbf{w}^H \mathbf{h}|^2] - |\mathbb{E}[\mathbf{w}^H \mathbf{h}]|^2$ .

2) *Receive Beamformer Design*: In the short timescale, the global statistical CSI is assumed to be shared among the APs. With the antenna positions and array orientations optimized over the long timescale being fixed, the receive beamformer at the  $m$ -th AP is obtained by maximizing the ergodic sum rate in (10) based on the available CSI  $\hat{\mathbf{H}}_m$ . From problem (11), it can be observed that the receive beamformer for the  $k$ -th user's signal is determined solely by the  $k$ -th MSE term  $\mathbb{E}[e_k(\varpi_k)]$ . By defining  $\tilde{\mathbf{w}}_k \triangleq [\tilde{\mathbf{w}}_{k,1}^H, \tilde{\mathbf{w}}_{k,2}^H, \dots, \tilde{\mathbf{w}}_{k,M}^H]^H = \varpi_k^{\text{opt}} \mathbf{w}_k$  and  $\tilde{\mathbf{W}}_m = [\tilde{\mathbf{w}}_{1,m}, \tilde{\mathbf{w}}_{2,m}, \dots, \tilde{\mathbf{w}}_{K,m}]$ , the short-timescale optimization problem for the  $m$ -th AP, based on available CSI  $\hat{\mathbf{H}}_m$ , can be equivalently simplified from problem (11) as

$$\begin{aligned} \min_{\tilde{\mathbf{W}}_m} \sum_{k=1}^K \mathbb{E} \left[ \left\| \sum_{i \neq k} \mathbf{H}_i^H \tilde{\mathbf{w}}_{k,i} + \mathbf{H}_m^H \tilde{\mathbf{w}}_{k,m} - \mathbf{e}_k \right\|_2^2 \right. \\ \left. + \sigma^2 \left( \sum_{i \neq k} \|\tilde{\mathbf{w}}_{k,i}\|_2^2 + \|\tilde{\mathbf{w}}_{k,m}\|_2^2 \right) \right] \Bigg| \hat{\mathbf{H}}_m. \end{aligned} \quad (13)$$

Notably, as stated in **Remark 1**, the receive beamformers at the other APs should be treated as functions of random fading channels. Since the objective function in (13) is convex and continuously differentiable w.r.t.  $\tilde{\mathbf{w}}_{k,m}$ , the optimal solution can be characterized by the first-order optimality condition, i.e.,

$$\hat{\mathbf{H}}_m \left( \sum_{i \neq m} \mathbb{E}[\mathbf{H}_i^H \tilde{\mathbf{w}}_{k,i}] + \hat{\mathbf{H}}_m^H \tilde{\mathbf{w}}_{k,m} - \mathbf{e}_k \right) + \sigma^2 \tilde{\mathbf{w}}_{k,m} = 0. \quad (14)$$

Hence, letting  $\hat{\mathbf{G}}_m = (\hat{\mathbf{H}}_m \hat{\mathbf{H}}_m^H + \sigma^2 \mathbf{I}_N)^{-1} \hat{\mathbf{H}}_m$ , the optimal value of  $\tilde{\mathbf{w}}_{k,m}$  in problem (13) is derived as

$$\tilde{\mathbf{w}}_{k,m}^{\text{opt}} \left( \hat{\mathbf{H}}_m \right) = \hat{\mathbf{G}}_m \left( \mathbf{e}_k - \sum_{i \neq m} \mathbb{E}[\mathbf{H}_i^H \tilde{\mathbf{w}}_{k,i}] \right). \quad (15)$$

**Remark 2.** It should be emphasized that although (15) yields the real-time per-AP optimal receive beamformer under available CSI, its computation depends on the statistical distributions of the channels and associated receive beamformers at the other APs. Due to this interdependency, (15) effectively introduces an iteratively update rule analogous to alternating optimization procedure, in which the  $m$ -th AP's receive beamformer is optimized while the statistical distributions of the receive beamformers at the remaining APs are kept fixed. Therefore, it is useful to establish that this iterative procedure converges to a stationary point and to derive a closed-form expression for that stationary point. From the perspective of team theory, the authors in [2] rigorously proved that when all APs adopt (15) to design their receive beamformers, the resulting solution is the unique global optimum of the original problem in (10). Furthermore, the short-timescale optimization problem in (13) can be generalized to incorporate any level of available CSI. Specifically, when the available CSI corresponds to the global instantaneous CSI  $\hat{\mathbf{H}}$ , the problem reduces to a centralized beamformer design.

To further eliminate the interdependency among the receive beamformers of different APs in (15), a closed-form expression for the LMMSE beamformer satisfying (15) is given by

$$\tilde{\mathbf{w}}_{k,m}^{\text{opt}} \left( \hat{\mathbf{H}}_m \right) = \hat{\mathbf{G}}_m \mathbf{c}_{k,m}, \quad \forall m, \quad (16)$$

where  $\mathbf{c}_k = [\mathbf{c}_{k,1}^T, \mathbf{c}_{k,2}^T, \dots, \mathbf{c}_{k,M}^T]^T \in \mathbb{C}^{KM \times 1}$  represents a set of long-timescale parameters that facilitate all APs to locally process the received signals from the  $k$ -th user. These parameters are determined by the statistical CSI and calculated as [2]

$$\mathbf{c}_k = (\text{blkdiag}(\mathbf{U} - \mathbf{V}) + \mathbf{U}^T \mathbf{V})^{-1} \mathbf{U}^T \mathbf{e}_k, \quad (17)$$

where  $\mathbf{V} = \mathbb{E}\{[\mathbf{H}_1^H \mathbf{G}_1, \mathbf{H}_2^H \mathbf{G}_2, \dots, \mathbf{H}_M^H \mathbf{G}_M]\} \in \mathbb{C}^{K \times KM}$  and  $\mathbf{U} = [\mathbf{I}_K, \mathbf{I}_K, \dots, \mathbf{I}_K] \in \mathbb{R}^{K \times KM}$ . The proof of the existence and uniqueness of  $\mathbf{c}_k$  is provided in Appendix V. By substituting (16) and (17) into (15), it follows directly that (16) constitutes an optimal solution for (15). Finally, since problem

(11) w.r.t. the receive beamformers is an unconstrained optimization problem and the fact of  $R_k^{\text{UatF}}(\tilde{\mathbf{w}}_k) = R_k^{\text{UatF}}(\mathbf{w}_k)$ , both  $\mathbf{w}_k$  and  $\tilde{\mathbf{w}}_k$  are locally optimal beamformers, resulting in the same ergodic sum rate. Therefore, we can directly update the beamformer using (16).

### B. Long-timescale Antenna Reconfiguration

In the long-timescale design, the receive beamformers based on the instantaneous CSI are regarded as functions of random CSI. By substituting the optimized receive beamformer in (16) into (8) and defining  $\mathbf{G} = \text{blkdiag}[\mathbf{G}_1, \mathbf{G}_2, \dots, \mathbf{G}_M]$ , the corresponding long-timescale subproblem w.r.t antenna positions and array orientations is formulated as

$$\max_{\mathbf{t}, \mathbf{r}} \mathbb{E} \left[ \underbrace{\sum_{k=1}^K \log_2 \left( 1 + \frac{|\mathbf{c}_k^H \mathbf{G}^H \mathbf{h}_k|^2}{\sum_{j \neq k} |\mathbf{c}_k^H \mathbf{G}^H \mathbf{h}_j|^2 + \sigma^2 \|\mathbf{G} \mathbf{c}_k\|_2^2} \right)}_{g\{\mathbf{H}(\mathbf{t}, \mathbf{r}), \mathbf{c}\}} \right] \quad (18a)$$

$$\text{s.t. (8b), (8c),} \quad (18b)$$

where  $\mathbf{c} = [\mathbf{c}_1^T, \mathbf{c}_2^T, \dots, \mathbf{c}_K^T]^T \in \mathbb{C}^{K^2 M \times 1}$  denotes the long-timescale parameter, with  $\mathbf{c}_k$  given by (17). It should be emphasized that the optimal long-timescale parameter  $\mathbf{c}$  given in (17) is determined by the statistical CSI, and thus implicitly depends on the antenna positions  $\mathbf{t}$  and array orientations  $\mathbf{r}$ . This interdependency induces strong coupling among  $\mathbf{t}$ ,  $\mathbf{r}$ , and  $\mathbf{c}$  in the objective function (18a), making the long-timescale optimization problem difficult to solve directly. To address this coupling, the sampled average approximation (SAA) is commonly employed to approximate the long-timescale parameter and the ergodic sum rate of all users via averaging over multiple random channel realizations [26], [27], [37], [39]. However, achieving sufficiently accurate approximation requires extensive sampling, which substantially increases the computational complexity in large-scale cell-free MIMO systems.

Given this challenge, it is necessary to develop an efficient optimization framework that can jointly address the interdependency among variables and reduce the computational burden. Although the optimal long-timescale parameter  $\mathbf{c}$  is formally characterized in (17), it involves an expectation operator embedded in a nonlinear function, which renders the problem analytically intractable. It is worth noting that the optimal  $\mathbf{c}$  is independent of the instantaneous CSI. This observation naturally motivates a centralized computation of

$\mathbf{c}$  at the CPU, followed by distributing it to all APs. At the AP level, each AP then determines its receive beamformer by combining the locally available instantaneous CSI with the provided long-term parameter  $\mathbf{c}$ . Therefore, to render the problem in (18) tractable, we treat  $\mathbf{c}$  as an auxiliary variable at the CPU. This relaxation leads to a computationally feasible yet suboptimal solution and converts the original problem in (18) into the following subproblem:

$$\begin{aligned} & \max_{\mathbf{t}, \mathbf{r}, \mathbf{c}} \mathbb{E} [g\{\mathbf{H}(\mathbf{t}, \mathbf{r}), \mathbf{c}\}] \\ & \text{s.t. (8b), (8c).} \end{aligned} \quad (19)$$

The coupled variables and expectation still lead to stochasticity and non-concavity of problem (19). As discussed above, to further decouple and then efficiently optimize these variables, the CSSCA framework is employed. In this framework, the original problem is iteratively addressed through a series of concave surrogate functions. In particular, the surrogate-function structure enables natural decoupling among different optimization variables, allowing them to be separately updated within each iteration. This facilitates online optimization while maintaining fast convergence and high computational efficiency [46], which will be detailed later.

The CSSCA procedure is described as follows. Recalling the channel model in (5), it is noteworthy that only  $\Psi \triangleq \{\{\{\psi_{k,l,m}\}_{m=1}^M\}_{l=1}^{L_k}\}_{k=1}^K$  are random variables. In the  $s$ -th iteration, a set of channel realization  $\Psi^s$  is realized to update the surrogate function  $\bar{f}^s(\mathbf{t}^s, \mathbf{r}^s, \Psi^s)$ , which can be regarded as a concave approximation of the objective function in (19) to calculate the long-timescale parameter, antenna positions, and array orientations in the next iteration.

Specifically, we adopt the smooth surrogate function construction proposed in [46], which can be viewed as a convex approximation of  $g\{\mathbf{H}(\mathbf{t}, \mathbf{r}), \mathbf{c}\}$  and is constructed as

$$\bar{f}^s(\mathbf{t}, \mathbf{r}, \mathbf{c}, \Psi^s) = f^s + f_{\mathbf{t}}^s(\mathbf{t}) + f_{\mathbf{r}}^s(\mathbf{r}) + f_{\mathbf{c}}^s(\mathbf{c}), \quad (20)$$

where  $f^s$  is an iterative average measure of the objective function in (19), which is given by

$$f^s = \frac{1}{s} \sum_{u=1}^s g\{\mathbf{H}(\mathbf{t}^s, \mathbf{r}^s, \Psi^u), \mathbf{c}^s\}. \quad (21)$$

$f_{\mathbf{t}}^s(\mathbf{t})$ ,  $f_{\mathbf{r}}^s(\mathbf{r})$ , and  $f_{\mathbf{c}}^s(\mathbf{c})$  are given by

$$f_{\mathbf{v}}^s(\mathbf{v}) = \text{Re} \left\{ (\mathbf{f}_{\mathbf{v}}^s)^H (\mathbf{v} - \mathbf{v}^s) + \tau_{\mathbf{v}} \|\mathbf{v} - \mathbf{v}^s\|_2^2 \right\}, \quad (22) \\ \mathbf{v} \in \{\mathbf{t}, \mathbf{r}, \mathbf{c}\},$$

where  $\{\tau_{\mathbf{v}}\}_{\mathbf{v} \in \{\mathbf{t}, \mathbf{r}, \mathbf{c}\}}$  are negative constants. The first and second terms in (22) are derived from the linearization of

$$\nabla_{\mathbf{c}_k} g(\mathbf{t}, \mathbf{r}, \mathbf{c}, \Psi) = \frac{1}{\ln 2} \left( \frac{\mathbf{G}^H \sum_{j=1}^K \mathbf{h}_j \mathbf{h}_j^H \mathbf{G} \mathbf{c}_k + \sigma^2 \mathbf{G}^H \mathbf{G} \mathbf{c}_k}{\sum_{j=1}^K |\mathbf{c}_k^H \mathbf{G}^H \mathbf{h}_j|^2 + \sigma^2 \|\mathbf{G} \mathbf{c}_k\|_2^2} - \frac{\mathbf{G}^H \sum_{j \neq k} \mathbf{h}_j \mathbf{h}_j^H \mathbf{G} \mathbf{c}_k + \sigma^2 \mathbf{G}^H \mathbf{G} \mathbf{c}_k}{\sum_{j \neq k} |\mathbf{c}_k^H \mathbf{G}^H \mathbf{h}_j|^2 + \sigma^2 \|\mathbf{G} \mathbf{c}_k\|_2^2} \right), \quad 1 \leq k \leq K. \quad (24)$$

the sampled objective function and the proximal regularization term, respectively. For notation simplicity, denote  $g(\mathbf{t}, \mathbf{r}, \mathbf{c}, \Psi) \triangleq g\{\mathbf{H}(\mathbf{t}, \mathbf{r}, \Psi), \mathbf{c}\}$ . The term  $\mathbf{f}_v^s$  approximates the first-order gradient of the objective function in (19) w.r.t. the variable  $\mathbf{v}$  and can be calculated recursively as

$$\mathbf{f}_v^s = (1 - \rho^s) \mathbf{f}_v^{s-1} + \rho^s \nabla_{\mathbf{v}} g(\mathbf{t}^s, \mathbf{r}^s, \mathbf{c}^s, \Psi^s), \mathbf{v} \in \{\mathbf{t}, \mathbf{r}, \mathbf{c}\}, \quad (23)$$

where  $f^{-1} \triangleq 0$  and  $\{\rho^s \in (0, 1]\}$  is a decreasing sequence such that  $\lim_{s \rightarrow \infty} \rho^s = 0$ ,  $\lim_{s \rightarrow \infty} \sum_s \rho^s \rightarrow \infty$ , and  $\lim_{s \rightarrow \infty} \sum_s (\rho^s)^2 \leq \infty$ . These conditions confirm the convergence of the proposed CSSCA procedure. The gradient of  $g(\mathbf{t}, \mathbf{r}, \mathbf{c}, \Psi)$  w.r.t.  $\mathbf{c}$  can be derived in closed form, as shown in (24) at the bottom of the previous page. Moreover, the gradients w.r.t.  $\mathbf{t}$  and  $\mathbf{r}$  are computed numerically. Specifically, the gradient w.r.t.  $\mathbf{r}$  is given by

$$[\nabla_{\mathbf{r}} g(\mathbf{t}^s, \mathbf{r}^s, \mathbf{c}^s, \Psi^s)]_i = \lim_{\varepsilon \rightarrow 0} \frac{g(\mathbf{t}^s, \mathbf{r}^s + \varepsilon \mathbf{e}_i, \mathbf{c}^s, \Psi^s) - g(\mathbf{t}^s, \mathbf{r}^s, \mathbf{c}^s, \Psi^s)}{\varepsilon}, 1 \leq i \leq 3M, \quad (25)$$

and the gradient w.r.t.  $\mathbf{t}$  can be obtained in a similar manner. Then, according to the CSSCA procedure [46], the optimization problem in the  $s$ -th iteration is recast into

$$\max_{\mathbf{t}, \mathbf{r}, \mathbf{c}} \bar{f}^s(\mathbf{t}, \mathbf{r}, \mathbf{c}, \Psi^s) \quad (26a)$$

$$\text{s.t. (8b), (8c).} \quad (26b)$$

Given that the decoupled construction of surrogate functions, problem (26) can be equivalently decoupled into three subproblems. Since the surrogate objective functions in (22) are convex quadratic and each subproblem is either unconstrained or subject to linear constraints, the unique solution for each can be determined in closed-form. Specifically, the optimal solution  $\{\bar{\mathbf{t}}^s, \bar{\mathbf{r}}^s, \bar{\mathbf{c}}^s\}$  is derived by projecting the unconstrained stationary point of the quadratic function onto its respective feasible region, i.e.,

$$\bar{\mathbf{t}}^s = \underset{\{\mathbf{t}_{m,n} \in \mathcal{T}_{m,n}\}_{\forall m,n}}{\operatorname{argmax}} \bar{f}_{\mathbf{t}}^s(\mathbf{t}) = \mathcal{B}_{\mathbf{t}} \left\{ \mathbf{t}^s - \frac{\mathbf{f}_{\mathbf{t}}^s}{2\tau_{\mathbf{t}}} \right\}, \quad (27)$$

$$\bar{\mathbf{r}}^s = \underset{\{\mathbf{r}_m \in \mathcal{R}\}_{\forall m}}{\operatorname{argmax}} \bar{f}_{\mathbf{r}}^s(\mathbf{r}) = \mathcal{B}_{\mathbf{r}} \left\{ \mathbf{r}^s - \frac{\mathbf{f}_{\mathbf{r}}^s}{2\tau_{\mathbf{r}}} \right\}, \quad (28)$$

$$\bar{\mathbf{c}}^s = \underset{\mathbf{c}}{\operatorname{argmax}} \bar{f}_{\mathbf{c}}^s(\mathbf{c}) = \mathbf{c}^s - \frac{\mathbf{f}_{\mathbf{c}}^s}{2\tau_{\mathbf{c}}}. \quad (29)$$

$\mathcal{B}_{\mathbf{t}}\{\mathbf{t}\}$  is a boundary projection function which ensures each element of the vectors  $\mathbf{t}$  being projected into its feasible region, which is given by

$$[\mathcal{B}_{\mathbf{t}}\{\mathbf{t}\}]_i = \begin{cases} [\mathbf{t}]_i^L, & \text{if } [\mathbf{t}]_i \leq [\mathbf{t}]_i^L, \\ [\mathbf{t}]_i, & \text{if } [\mathbf{t}]_i^L < [\mathbf{t}]_i \leq [\mathbf{t}]_i^U, \\ [\mathbf{t}]_i^U, & \text{if } [\mathbf{t}]_i^U < [\mathbf{t}]_i, \end{cases} \quad (30)$$

where  $[\mathbf{t}]_i^L$  and  $[\mathbf{t}]_i^U$  denote the lower and upper bounds on the  $i$ -th element of  $\mathbf{t}$ , respectively, as specified by the movable region  $\{\{\mathcal{T}_{m,n}\}_{n=1}^N\}_{m=1}^M$ . The boundary function of the array

---

**Algorithm 1** CSSCA-based Two-timescale Design

---

**Input:**  $\mathbf{t}^0, \mathbf{r}^0, \mathbf{c}^0$ .

**Output:**  $\mathbf{t}, \mathbf{r}, \mathbf{c}$ .

- 1: Set iteration index  $s = 0$ .
- 2: **repeat**
- 3: Generate a sample of random path coefficients  $\Psi^s$ .
- 4: Obtain the short-timescale receive beamformers  $\mathbf{w}_{k,m}\{\mathbf{H}(\mathbf{t}^s, \mathbf{r}^s, \Psi^s), \mathbf{c}^s\}$  according to (16).
- 5: Construct the surrogate function  $\bar{f}^s(\mathbf{t}, \mathbf{r}, \mathbf{c}, \Psi^s)$  according to (20).
- 6: Obtain the stationary points  $\bar{\mathbf{t}}^s, \bar{\mathbf{r}}^s$ , and  $\bar{\mathbf{c}}^s$  according to (27), (28), and (29).
- 7: Update the long-timescale variables  $\mathbf{t}^{s+1}, \mathbf{r}^{s+1}$ , and  $\mathbf{c}^{s+1}$  according to (31), (32), and (33).
- 8: Set  $s = s + 1$ .
- 9: **until** the maximum iteration number  $s_{\max}$  is reached.

---

orientations,  $\mathcal{B}_{\mathbf{r}}\{\mathbf{r}\}$ , is defined in a similar manner, with the rotatable region predetermined by  $\mathcal{R}$ .

Finally, given  $\bar{\mathbf{t}}^s, \bar{\mathbf{r}}^s$ , and  $\bar{\mathbf{c}}^s$ , the antenna positions, array orientations, and long-timescale parameter are updated in the next iteration as

$$\mathbf{t}^{s+1} = (1 - \gamma^s) \mathbf{t}^s + \gamma^s \bar{\mathbf{t}}^s, \quad (31)$$

$$\mathbf{r}^{s+1} = (1 - \gamma^s) \mathbf{r}^s + \gamma^s \bar{\mathbf{r}}^s, \quad (32)$$

$$\mathbf{c}^{s+1} = (1 - \gamma^s) \mathbf{c}^s + \gamma^s \bar{\mathbf{c}}^s, \quad (33)$$

respectively, where the sequence  $\gamma^s$  follows the same properties of  $\rho^s$  and satisfies  $\lim_{s \rightarrow \infty} \frac{\gamma^s}{\rho^s} = 0$  [46].

**Remark 3.** As iteration number  $s$  increases, the term  $\mathbf{f}_v^s$  in (23) approximates the first-order gradient of the objective function in (19) with increasing accuracy. Notably, the convex surrogate functions are constructed as first-order Taylor expansions of the original non-concave functions, augmented by a quadratic regularization term to ensure uniform strong convexity. Based on this construction of surrogate functions, the updates of  $\{\mathbf{t}^s, \mathbf{r}^s, \mathbf{c}^s\}$  can be interpreted as the estimation of stationary solutions for the original problem in (19).

The overall two-timescale workflow is summarized in Algorithm 1. The convergence is guaranteed since the iteratively updated solutions converge almost surely to stationary points of the original problem (19) as the iteration index  $s \rightarrow \infty$ . A detailed proof can be found in Theorem 1 of [46]. The computational complexity of Algorithm 1 is primarily attributed to the calculation of the gradients  $\nabla_{\mathbf{v}} g(\mathbf{t}^s, \mathbf{r}^s, \mathbf{c}^s, \Psi^s), \mathbf{v} \in \{\mathbf{t}, \mathbf{r}, \mathbf{c}\}$ . The corresponding computational orders are  $\mathcal{O}(MN^2(\sum_k \sum_m L_{k,m} + M(N^2 + KN + K^2)))$ ,  $\mathcal{O}(N^2(\sum_k \sum_m L_{k,m} + M(N^2 + KN + K^2)))$ , and  $\mathcal{O}(K^3 MN)$ , respectively. Considering the dominant operations, the overall computational complexity of Algorithm 1 is given by  $\mathcal{O}(s_{\max}(MN^2(\sum_k \sum_m L_{k,m} + M(N^2 + KN + K^2))))$ . It is worth noting that this long-timescale optimization is executed only when the channel statistical characteristics

vary significantly. As a result, the proposed framework effectively reduces the implementation complexity and overhead, in contrast to conventional designs that rely on instantaneous CSI and require frequent update of antenna positions and array orientations.

#### IV. NUMERICAL RESULTS

##### A. Simulation Setup

TABLE I  
SIMULATION PARAMETERS

Parameter	Value
Carrier frequency	$f_c = 20$ GHz
Wavelength	$\lambda = 0.015$ m
Number of APs	$M = 10$
Number of antennas per AP	$N = 6$
Number of users	$K = 10$
Number of paths	$L = 6$
Rician factor	$\kappa = 10$ dB
Movable region size for each antenna	$\lambda \times \lambda$
Rotatable range for each array	$[-30^\circ, 30^\circ]$
Average noise power	$-70$ dBm
Searching step size	$\hat{\kappa}_c = \hat{\kappa}_r = 10$
Error tolerance	$\varepsilon = 10^{-3}$
Maximum number of iterations	$s_{\max} = 100$

In this section, numerical results are provided to evaluate the performance of the proposed two-timescale decentralized design for the 6DMA-aided cell-free MIMO system. We consider the APs are deployed uniformly along a ring of radius 140 m to serve the users distributed within a circular area of radius 120 m. The path-loss is computed based on the 3GPP Urban Microcell model [47], given by

$$\rho_{k,m} = -22.7 - 36.7 \lg \left( \frac{d_{k,m}}{1 \text{ m}} \right) - 26 \lg \left( \frac{f_c}{1 \text{ GHz}} \right) \text{ [dB]},$$

where  $d_{k,m}$  denotes the distance between the  $k$ -th user and the  $m$ -th AP, with a height difference of 10 m. The numbers of received paths between all APs and users are assumed to be identical, i.e.,  $L_{k,m} = L$ . The fading coefficients follow  $\psi_{k,1,m} \sim \mathcal{CN}(0, (\kappa \rho_{k,m}) / (\kappa + 1))$  and  $\psi_{k,l,m} \sim \mathcal{CN}(0, \rho_{k,m} / ((\kappa + 1)(L - 1)))$  for  $\forall l \neq 1$ , where the Rician factor  $\kappa$  characterizes the relative strength of the LoS component. The AoAs of the non-LoS (NLoS) paths for each AP are generated according to a joint probability density function  $f(\theta_{k,l,m}, \phi_{k,l,m}) = \frac{\sin \theta_{k,l,m}}{2\pi}$  with  $\theta_{k,l,m} \in [0, \pi]$  and  $\phi_{k,l,m} \in [0, \pi]$  [11]. For each AP, the initial spacing between adjacent antennas is set to  $5\lambda$ . All antennas share the same movable region relative to their initial positions, and all arrays have the same allowable pitch, roll, and yaw rotation ranges. The performance is evaluated through 200 independent realizations of user distributions and channel coefficients. For each realization, the ergodic sum rate of all users is obtained using  $s_{\max} = 100$  stochastic samples to execute Algorithm 1. In the short timescale, the expectations of the stochastic parameters are approximated using the SAA method. The parameters for CSSCA algorithm are set to  $\rho^s = \frac{1}{(1+s)^{0.9}}$  and  $\gamma^s = \frac{15}{15+s}$  [46].

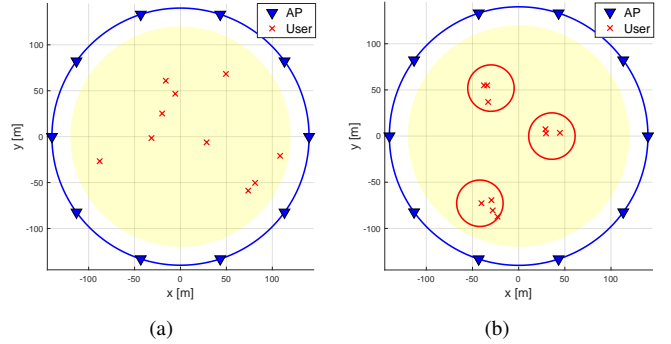


Fig. 4. The simulation setups under different user distributions. (a) Users are uniformly distributed within serving area. (b) Users are densely concentrated around three hotspots.

##### B. User Distribution and Baseline Schemes

To investigate the effectiveness of antenna movement for interference mitigation and performance enhancement under different levels of inter-user interference, particularly in the presence of dominant LoS components, the proposed CSSCA algorithm (labeled as **Proposed LMMSE with 6DMA**) is evaluated in two specific communication scenarios, as illustrated in Fig. 4, where users are either uniformly distributed within the serving area or densely concentrated around three hotspots. To verify the effectiveness of the proposed 6DMA-aided cell-free system, the performance of Algorithm 1 is compared with the following baselines:

- **Centralized MMSE with FPA:** All APs are equipped with FPAs and upload their acquired CSI to the CPU, which jointly decodes the received signals based on the MMSE receive beamformer  $\mathbf{W} = (\mathbf{H}\mathbf{H}^H + \sigma^2 \mathbf{I}_{MN})^{-1} \mathbf{H}$  [48]. The FPAs within each AP are arranged with an inter-element spacing of  $5\lambda$ , which is the same as the initial position of the 6DMA.
- **LMMSE with FPA:** All APs are equipped with FPAs and independently computes its LMMSE receive beamformer. The long-timescale parameter  $\mathbf{c}$  is obtained by SAA method over the long timescale.
- **LMMSE with flexible position:** The decentralized cell-free system executes Algorithm 1 while keeping the array orientations of all APs fixed.
- **LMMSE with flexible orientation:** The decentralized cell-free system executes Algorithm 1 while keeping the antenna positions of all APs fixed.

##### C. Algorithm Convergence

Fig. 5 illustrates the convergence behavior of the proposed CSSCA-based algorithm under different flexibilities of antenna movement and array rotation. As observed, although the performance curves exhibit fluctuations, the ergodic sum rate almost surely converges to a steady value as the iteration number increases, which verifies the feasibility of Algorithm 1.

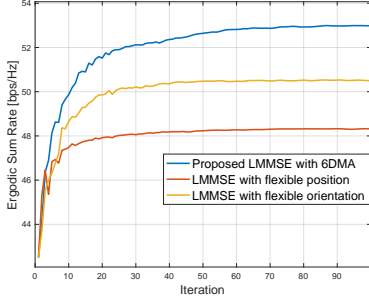


Fig. 5. Convergence of Algorithm 1 under uniform user distribution.

Specifically, all three benchmarks achieve most of their performance gain within 50 iterations, indicating that the proposed algorithm features fast convergence and high computational efficiency.

#### D. Uniform User Distribution

In this subsection, we consider the scenario where the users are uniformly distributed within the serving area, as illustrated in Fig. 4(a), and evaluate the performance w.r.t. different system parameters.

Fig. 6(a) presents the empirical cumulative distribution function (CDF) of the ergodic sum rate obtained from multiple independent realizations of quasi-static AoAs and users locations. It is observed that the proposed 6DMA-aided scheme outperforms the FPA and other less flexible counterparts. This is because the array rotation focuses energy toward directions with strong channel paths, thereby exploiting angular DoFs more effectively and improving the overall ergodic sum rate. Interestingly, it shows that under a uniform user distribution with moderate inter-user interference, the proposed scheme approaches the performance of the centralized MMSE baseline and even surpasses it in specific channel realizations. This result highlights that antenna movement enables cell-free MIMO systems to better adapt to complex propagation environments and significantly enhance communication performance.

Fig. 6(b) illustrates the ergodic sum rate of all users versus the movable region size. It is observed that the ergodic sum rate of the 6DMA scheme increases with the region size and eventually converge. These results demonstrate that enlarging the movable region provides additional DoFs for reducing channel correlation among users, thereby efficiently mitigating inter-user interference. Moreover, a bounded per-antenna movement region within three to four wavelengths is sufficient for the cell-free MIMO decentralized architecture to reap most of the performance gain with a moderate system overhead, and can even approach the performance of the centralized MMSE baseline.

Fig. 6(c) shows the ergodic sum rate of all users versus the rotatable range. The ergodic sum rate achieved by the proposed 6DMA scheme increases with the rotation range until reaching a constant. This suggests that a moderate rotation range is sufficient for each AP to orient its array toward the statistically

dominant propagation direction and concentrate the radiated energy accordingly. Furthermore, in cell-free MIMO systems with distributed deployment of APs, the wider signal coverage leads to more stronger LoS components, which enables 6DMA to more accurately capture statistically favorable propagation directions, thereby further improving communication performance.

Fig. 6(d) depicts the performance gains achieved by 6DMA under different strength levels of LoS components. Note that small and large Rician factors represent weaker and stronger LoS components, respectively. Specifically, when  $\kappa = -10$  dB, the LoS path is weaker than any other NLoS paths, corresponding to LoS-blocked scenarios. Under this condition, the performance gains of 6DMA are severely limited, since there is no clearly dominant propagation direction. In contrast,  $\kappa = 20$  dB implies that the multi-path channel approximates a pure LoS channel. In this case, the results reveal that the performance gain from 6DMA becomes more pronounced and can even outperform the MMSE baseline due to the existence of an apparently dominant propagation direction, which allows more effective inter-user interference mitigation and radiated energy concentration.

It should be emphasized that although the centralized scheme achieves a superior performance owing to global CSI availability and instantaneous joint signal processing, it imposes considerable computational and CSI-exchange overheads, thereby limiting network scalability. In contrast, the proposed decentralized framework offers a more practical balance between performance and implementation complexity.

#### E. Concentrated User Distribution

In this subsection, we consider the scenario where the users are concentrated around three predefined hotspots, as illustrated in Fig. 4(b), and evaluate the performance improvement trends w.r.t. different system parameters.

Fig. 7(a) shows the CDF of the ergodic sum rate of all users. Under a concentrated user distribution, although the proposed scheme maintains performance superiority over other less flexible benchmarks, its performance gap to the MMSE baseline becomes substantial. The reason behind is that the channels between the densely distributed users and each AP are highly correlated, especially in the presence of dominant LoS components, resulting in severe inter-user interference. Under such conditions, it becomes difficult for each AP with a limited number of antennas and LMMSE-based receive beamformer to completely suppress the interference.

The relationships between the ergodic sum rate of all users and the movable region size, rotation range, and Rician factor are presented in Figs. 7(b), 7(c), and 7(d), respectively. It can be observed that the proposed 6DMA scheme achieves higher ergodic sum rates compared with the FPA and other less flexible counterparts, consistent with the conclusions drawn in Section IV-D, thereby verifying the effectiveness of the proposed framework. However, as shown in the three subfigures, the performance improvements brought by 6DMA

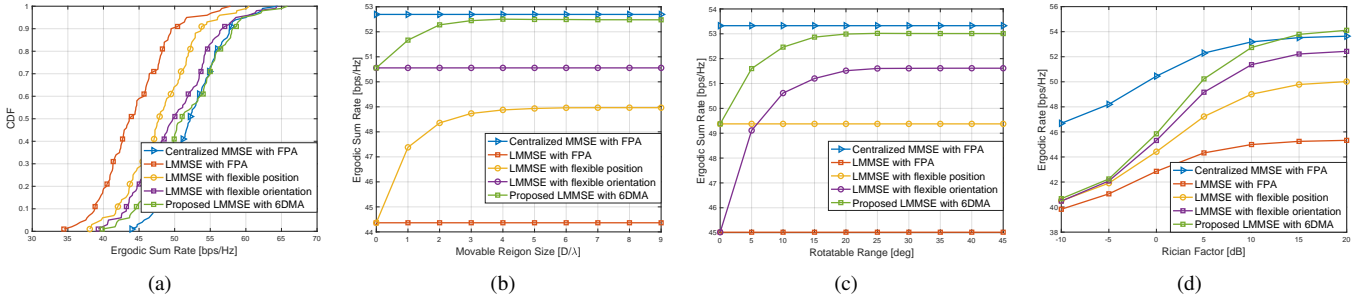


Fig. 6. The performance comparison among different schemes with users uniformly distributed within the serving area. (a) The CDF of the ergodic sum rate of all users. (b) The ergodic sum rate of all users versus the movable region size. (c) The ergodic sum rate of all users versus the rotatable range. (d) The ergodic sum rate of all users versus the Rician factor.

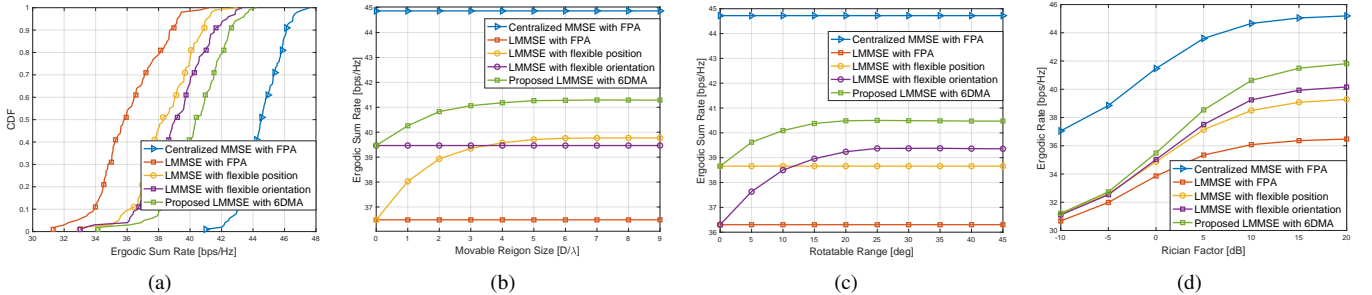


Fig. 7. The performance comparison among different schemes with users concentrated around three hotspots. (a) The CDF of the ergodic sum rate of all users. (b) The ergodic sum rate of all users versus the movable region size. (c) The ergodic sum rate of all users versus the rotatable range. (d) The ergodic sum rate of all users versus the Rician factor.

are significantly reduced compared with those under the uniform user distribution scenario. This is because, in the dense user distribution case, the channels of users located within the same hotspot are highly correlated, which is difficult to decorrelate using the limited number of antennas available at each AP. Such limitation restricts the exploitation of additional DoFs provided by antenna movement, thereby limiting further performance enhancement.

In addition, it is noteworthy that, under this dense-user condition, the performance improvements contributed individually by antenna position and array orientation become comparable. This observation can be explained as follows. Antenna position optimization helps mitigate channel correlation by providing higher spatial resolution in the angular domain, enabling better separation of users located in similar directions. On the other hand, antenna orientation optimization primarily enhances directional energy focusing toward the statistically dominant propagation paths. Therefore, jointly considering both antenna position and orientation optimization allows the system to combine their complementary advantages, further improving the overall communication performance of 6DMA-aided cell-free MIMO systems.

## V. CONCLUSION

This paper has investigated a 6DMA-aided cell-free system for uplink multi-user communications. To mitigate the overhead caused by frequent antenna movement and CSI exchange

among distributed APs, a two-timescale decentralized optimization framework was developed to effectively maximize the ergodic sum rate of all users. In the short timescale, the optimal LMMSE receive beamformer design rule was derived, enabling each AP to design its receive beamformer based on local instantaneous CSI and global statistical CSI. In the long timescale, the CSSCA framework was employed, which iteratively constructs a sequence of surrogate problems to approximate the original stochastic objective function. This approach effectively decouples the optimization variables and enables their updates in parallel, thereby yielding computationally efficient solutions. Numerical results demonstrated that the proposed 6DMA-aided cell-free system significantly outperforms the conventional FPA and other antenna movement schemes with less flexibility. Notably, under specific practical conditions, the proposed 6DMA scheme can achieve a performance comparable to and even better than the centralized MMSE baseline with FPAs. Moreover, the results highlighted that the performance improvements are more pronounced with sparse user distribution. Beyond the scope of this work, other fronthaul architectures such as unidirectional, tree, or star topologies, which enable enhanced CSI sharing among APs, as well as the corresponding decentralized antenna movement designs, can further exploit the potential of cell-free networks. These directions are worth being explored in future work.

## APPENDIX

### DERIVATION OF (17)

Substituting the closed-form receive beamformer (16) into the per-AP optimality condition (15) yields

$$\hat{\mathbf{G}}_m \mathbf{c}_{k,m} - \hat{\mathbf{G}}_m \left( \mathbf{e}_k - \sum_{i \neq m} \mathbb{E} [\mathbf{H}_i^H \mathbf{G}_i \mathbf{c}_{k,i}] \right) = 0, \forall m. \quad (34)$$

Since the equality holds for all realizations of the local CSI  $\hat{\mathbf{G}}_m$ , we can obtain that

$$\mathbf{c}_{k,m} + \sum_{i \neq m} \mathbb{E} [\mathbf{H}_i^H \mathbf{G}_i] \mathbf{c}_{k,i} = \mathbf{e}_k, \forall m. \quad (35)$$

Stacking (35) over  $m$  and using the definitions of the block matrices  $\mathbf{U}$  and  $\mathbf{V}$  gives the linear system

$$(\text{blkdiag}(\mathbf{U} - \mathbf{V}) + \mathbf{U}^T \mathbf{V}) \mathbf{c}_k = \mathbf{U}^T \mathbf{e}_k. \quad (36)$$

Therefore, it suffices to show that  $(\text{blkdiag}(\mathbf{U} - \mathbf{V}) + \mathbf{U}^T \mathbf{V})$  is nonsingular. According to Woodbury matrix identity, i.e.,  $(\mathbf{I} + \mathbf{AB})^{-1} = \mathbf{I} - \mathbf{A}(\mathbf{I} + \mathbf{BA})^{-1}\mathbf{B}$ , where  $\mathbf{A}$  and  $\mathbf{B}$  are arbitrary matrices, this is equivalent to proving that  $\mathbf{I}_K + \mathbf{V}(\text{blkdiag}(\mathbf{U} - \mathbf{V}))^{-1}\mathbf{U}^T$  is invertible. Let  $\mathbf{V}_i = \mathbb{E}[\mathbf{H}_i^H \mathbf{G}_i]$ ,  $\forall 1 \leq i \leq M$ , we first prove that  $\mathbf{I}_K - \mathbf{V}_i$  is invertible for all  $i$ , which is given by

$$\begin{aligned} \mathbf{I}_K - \mathbf{V}_i &= \mathbb{E}[\mathbf{I}_K - \mathbf{H}_i^H \mathbf{G}_i] \\ &= \mathbb{E} \left[ \mathbf{I}_K - \mathbf{H}_i^H (\mathbf{H}_i \mathbf{H}_i^H + \sigma^2 \mathbf{I}_N)^{-1} \mathbf{H}_i \right] \\ &\stackrel{(b)}{=} \mathbb{E} \left[ \left( \mathbf{I}_K + \frac{1}{\sigma^2} \mathbf{H}_i^H \mathbf{H}_i \right)^{-1} \right], \end{aligned} \quad (37)$$

where equality (b) is obtained by applying the Woodbury matrix identity. Since expectation preserves positive definiteness, it then follows that  $\mathbf{I}_K - \mathbf{V}_i$  is positive definite and invertible. Moreover, using the singular value decomposition, it can be shown that  $\mathbf{V}_i$  is invertible. Consequently, by exploiting the specific block structures of  $\mathbf{U}$  and  $\mathbf{V}$ , we obtain

$$\begin{aligned} \mathbf{I}_K + \mathbf{V}(\text{blkdiag}(\mathbf{U} - \mathbf{V}))^{-1} \mathbf{U}^T &\stackrel{(c)}{=} \mathbf{I}_K + \sum_{i=1}^M \mathbf{V}_i (\mathbf{I}_K - \mathbf{V}_i)^{-1} \\ &\stackrel{(d)}{=} \mathbf{I}_K + \sum_{i=1}^M \mathbf{P}_i^H \Sigma_i (\mathbf{I}_K - \Sigma_i)^{-1} \mathbf{P}_i, \end{aligned} \quad (38)$$

where (c) follows from  $[\mathbf{A}_1, \mathbf{A}_2, \dots, \mathbf{A}_N] \times [\mathbf{B}_1, \mathbf{B}_2, \dots, \mathbf{B}_N]^T = \sum_{i=1}^N \mathbf{A}_i \mathbf{B}_i^T$  with  $\mathbf{A}_i \in \mathbb{C}^{m \times n}$  and  $\mathbf{B}_i \in \mathbb{C}^{m \times n}$  being arbitrary matrices. The equation (d) is obtained from the unitary decomposition of the Hermitian matrix  $\mathbf{V}_i = \mathbf{P}_i^H \Sigma_i \mathbf{P}_i$ , with  $\mathbf{P}_i$  being a unitary matrix and  $\Sigma_i$  a diagonal matrix. Since both  $\mathbf{I}_K - \mathbf{V}_i$  and  $\mathbf{V}_i$  are positive definite, equation (38) further shows that  $\mathbf{I}_K + \mathbf{V}(\text{blkdiag}(\mathbf{U} - \mathbf{V}))^{-1} \mathbf{U}^T$  is positive definite and invertible.

Therefore, we have  $\mathbf{c}_k = (\text{blkdiag}(\mathbf{U} - \mathbf{V}) + \mathbf{U}^T \mathbf{V})^{-1} \mathbf{U}^T \mathbf{e}_k$ , which completes the derivation.

### REFERENCES

- [1] T. Demir, E. Björnson, and L. Sanguinetti, "Foundations of user-centric cell-free massive MIMO," *Foundations and Trends in Signal Process.*, 2021.
- [2] L. Miretti, E. Björnson, and D. Gesbert, "Team MMSE precoding with applications to cell-free massive MIMO," *IEEE Trans. Wireless Commun.*, vol. 21, no. 8, pp. 6242–6255, Aug. 2022.
- [3] N. Ul Ain, L. Miretti, and S. Stańczak, "On the optimal performance of distributed cell-free massive MIMO with LoS propagation," in *2025 IEEE Wireless Commun. Network. Conf. (WCNC)*, Milan, Italy, 2025, pp. 1–7.
- [4] L. Miretti, R. L. G. Cavalcante, and S. Stańczak, "Two-timescale joint power control and beamforming design with applications to cell-free massive MIMO," *IEEE Trans. Wireless Commun.*, early access, 2025.
- [5] N. Zhou, Z. Wang, C. Ma, Y. Huang, and Q. Shi, "Distributed precoder based on weighted MMSE with low complexity for massive MIMO systems," *IEEE Commun. Lett.*, vol. 29, no. 3, pp. 482–486, Mar. 2025.
- [6] Z. Hong, S. Xu, T. Li, C. Li, D. Wang, and X. You, "Robust cascaded team MMSE precoding for cell-free distributed downlink under hierarchical fronthaul," *IEEE Trans. Wireless Commun.*, vol. 23, no. 10, pp. 14515–14529, Oct. 2024.
- [7] Y. Zhang and T. Y. Al-Naffouri, "Enabling scalable distributed beamforming via networked LEO satellites towards 6G," *IEEE Trans. Wireless Commun.*, early access, 2025.
- [8] Y. Zhang, L. Eva, X. X. Zheng, C. Symeon, and T. Y. Al-Naffouri, "Decentralized cooperative beamforming for networked LEO satellites with statistical csi," *arXiv:2512.18890*, 2025.
- [9] L. Zhu, W. Ma, W. Mei, Y. Zeng, Q. Wu, B. Ning, Z. Xiao, X. Shao, J. Zhang, and R. Zhang, "A tutorial on movable antennas for wireless networks," *IEEE Commun. Surv. Tutor.*, early access, 2025.
- [10] L. Zhu and K.-K. Wong, "Historical review of fluid antenna and movable antenna," *arXiv:2401.02362*, 2024.
- [11] L. Zhu, W. Ma, and R. Zhang, "Modeling and performance analysis for movable antenna enabled wireless communications," *IEEE Trans. Wireless Commun.*, vol. 23, no. 6, pp. 6234–6250, Jun. 2024.
- [12] W. Ma, L. Zhu, and R. Zhang, "MIMO capacity characterization for movable antenna systems," *IEEE Trans. Wireless Commun.*, vol. 23, no. 4, pp. 3392–3407, Apr. 2024.
- [13] L. Zhu, W. Ma, B. Ning, and R. Zhang, "Movable-antenna enhanced multiuser communication via antenna position optimization," *IEEE Trans. Wireless Commun.*, vol. 23, no. 7, pp. 7214–7229, Jul. 2024.
- [14] L. Zhu, W. Ma, and R. Zhang, "Movable-antenna array enhanced beamforming: Achieving full array gain with null steering," *IEEE Commun. Letters*, vol. 27, no. 12, pp. 3340–3344, Dec. 2023.
- [15] L. Zhu, X. Pi, W. Ma, Z. Xiao, and R. Zhang, "Dynamic beam coverage for satellite communications aided by movable-antenna array," *IEEE Trans. Wireless Commun.*, vol. 24, no. 3, pp. 1916–1933, Mar. 2025.
- [16] H. Mao, L. Zhu, X. Pi, Z. Xiao, X.-G. Xia, and R. Zhang, "Robust design for movable-antenna array enabled UAV communications with jittering," *IEEE Wireless Commun. Letters*, early access, 2025.
- [17] Y. Zhang, Y. Zhang, L. Zhu, S. Xiao, W. Tang, Y. C. Eldar, and R. Zhang, "Movable antenna-aided hybrid beamforming for multi-user communications," *IEEE Trans. Veh. Technol.*, vol. 74, no. 6, pp. 9899–9903, Jun. 2025.
- [18] Z. Xiao, X. Pi, L. Zhu, X.-G. Xia, and R. Zhang, "Multiuser communications with movable-antenna base station: Joint antenna positioning, receive combining, and power control," *IEEE Trans. Wireless Commun.*, vol. 23, no. 12, pp. 19744–19759, Dec. 2024.
- [19] Z. Xiao, X. Pi, S. Cao, L. Zhu, Z. Gao, X.-G. Xia, and R. Zhang, "Fundamental models and signal processing for movable antenna-enhanced wireless communications and sensing," *arXiv:2511.05048*, 2025.
- [20] Y. Wu, D. Xu, D. W. K. Ng, W. Gerstacker, and R. Schober, "Globally optimal movable antenna-enabled multiuser communication: Discrete antenna positioning, power consumption, and imperfect CSI," *IEEE Trans. Commun.*, early access, 2025.
- [21] Q. Li, W. Mei, B. Ning, and R. Zhang, "Minimizing movement delay for movable antennas via trajectory optimization," in *Proc. IEEE Global Commun. Conf. (GLOBECOM)*, Cape Town, South Africa, Dec. 2024, pp. 1–6.
- [22] J. Ding, Z. Zhou, L. Zhu, Y. Zhao, B. Jiao, and R. Zhang, "Energy efficiency maximization for movable antenna communication systems," *IEEE Trans. Wireless Commun.*, early access, 2025.

[23] X. Chen, B. Feng, Y. Wu, D. W. Kwan Ng, and R. Schober, "Joint beamforming and antenna movement design for moveable antenna systems based on statistical CSI," in *Proc. IEEE Global Commun. Conf. (GLOBECOM)*, Kuala Lumpur, Malaysia, Dec. 2023, pp. 4387–4392.

[24] Y. Ye, L. You, J. Wang, H. Xu, K.-K. Wong, and X. Gao, "Fluid antenna-assisted MIMO transmission exploiting statistical CSI," *IEEE Commun. Letters*, vol. 28, no. 1, pp. 223–227, Jan. 2024.

[25] G. Hu, Q. Wu, G. Li, D. Xu, K. Xu, J. Si, Y. Cai, and N. Al-Dhahir, "Two-timescale design for movable antenna array-enabled multiuser uplink communications," *IEEE Trans. Veh. Technol.*, vol. 74, no. 3, pp. 5152–5157, Mar. 2025.

[26] G. Yan, L. Zhu, and R. Zhang, "Movable antenna aided multiuser communications: Antenna position optimization based on statistical channel information," *IEEE Trans. Wireless Commun.*, early access, 2025.

[27] X. Shao, Q. Jiang, and R. Zhang, "6D movable antenna based on user distribution: Modeling and optimization," *IEEE Trans. Wireless Commun.*, vol. 24, no. 1, pp. 355–370, Jan. 2025.

[28] X. Shao, R. Zhang, Q. Jiang, and R. Schober, "6D movable antenna enhanced wireless network via discrete position and rotation optimization," *IEEE J. Sel. Areas Commun.*, vol. 43, no. 3, pp. 674–687, Mar. 2025.

[29] Y. Zhang, Y. Zhang, L. Zhu, S. Xiao, W. Tang, Y. C. Eldar, and R. Zhang, "6DMA-aided hybrid beamforming with joint antenna position and orientation optimization," *arxiv:2412.17088*, 2024.

[30] T. Ren, X. Zhang, L. Zhu, W. Ma, X. Gao, and R. Zhang, "6-D movable antenna enhanced interference mitigation for cellular-connected uav communications," *IEEE Wireless Commun. Letters*, vol. 14, no. 6, pp. 1618–1622, Jun. 2025.

[31] H. Wang, X. Shao, B. Zheng, X. Shi, and R. Zhang, "Passive six-dimensional movable antenna (6DMA)-assisted multiuser communication," *IEEE Wireless Commun. Letters*, vol. 14, no. 4, pp. 1014–1018, Apr. 2025.

[32] X. Xiong, B. Zheng, W. Wu, X. Shao, L. Dai, M.-M. Zhao, and J. Tang, "Efficient channel estimation for rotatable antenna-enabled wireless communication," *IEEE Wireless Commun. Letters*, early access, 2025.

[33] X. Shao, L. Hu, Y. Sun, X. Li, Y. Zhang, J. Ding, X. Shi, F. Chen, D. W. K. Ng, and R. Schober, "Hybrid near-far field 6D movable antenna design exploiting directional sparsity and deep learning," *IEEE Trans. Wireless Commun.*, early access, 2025.

[34] X. Shao, W. Mei, C. You, Q. Wu, B. Zheng, C.-X. Wang, J. Li, R. Zhang, R. Schober, L. Zhu, W. Zhuang, and X. Shen, "A tutorial on six-dimensional movable antenna for 6G networks: Synergizing positionable and rotatable antennas," *IEEE Commun. Surv. Tutor.*, early access, 2025.

[35] X. Shao and R. Zhang, "6DMA enhanced wireless network with flexible antenna position and rotation: Opportunities and challenges," *IEEE Commun. Mag.*, vol. 63, no. 4, pp. 121–128, Apr. 2025.

[36] Z. Xiao, S. Cao, L. Zhu, Y. Liu, B. Ning, X.-G. Xia, and R. Zhang, "Channel estimation for movable antenna communication systems: A framework based on compressed sensing," *IEEE Trans. Wireless Commun.*, vol. 23, no. 9, pp. 11814–11830, Sep. 2024.

[37] X. Shi, X. Shao, B. Zheng, and R. Zhang, "6DMA-aided cell-free massive MIMO communication," *IEEE Wireless Commun. Lett.*, vol. 14, no. 5, pp. 1361–1365, May 2025.

[38] W. Wang, Y. Huang, X. Shao, and C. Zhang, "Aerial 6D movable antenna-enabled cell-free networks," *IEEE Trans. Veh. Technol.*, pp. 1–6, early access, 2025.

[39] X. Pi, L. Zhu, H. Mao, Z. Xiao, X.-G. Xia, and R. Zhang, "6D movable antenna enhanced multi-access point coordination via position and orientation optimization," *IEEE Trans. Wireless Commun.*, early access, 2025.

[40] A. Sayeed, "Deconstructing multiantenna fading channels," *IEEE Trans. Signal Process.*, vol. 50, no. 10, pp. 2563–2579, Oct. 2002.

[41] R. Bhagavatula, C. Oestges, and R. W. Heath, "A new double-directional channel model including antenna patterns, array orientation, and depolarization," *IEEE Trans. Veh. Technol.*, vol. 59, no. 5, pp. 2219–2231, Jun. 2010.

[42] 3GPP, "Study on channel model for frequencies from 0.5 to 100 Ghz," 3GPP, Tech. Rep. TR 138 901 V18.0.0 (2024-05), 2024.

[43] C. A. Balanis, *Antenna theory: analysis and design*. John Wiley & sons, 2016.

[44] T. L. Marzetta, E. G. Larsson, H. Yang, and H. Q. Ngo, *Fundamentals of massive MIMO*. Cambridge University Press, 2016.

[45] K. Shen and W. Yu, "Fractional programming for communication systems-part II: Uplink scheduling via matching," *IEEE Trans. Signal Process.*, vol. 66, no. 10, pp. 2631–2644, May 2018.

[46] A. Liu, V. K. N. Lau, and B. Kananian, "Stochastic successive convex approximation for non-convex constrained stochastic optimization," *IEEE Trans. Signal Process.*, vol. 67, no. 16, pp. 4189–4203, Aug. 2019.

[47] 3GPP, "Further advancements for E-UTRA physical layer aspects (release 9)," 3GPP, Tech. Rep. Tech. Rep. TS 36.814, Mar. 2017.

[48] Q. Shi, M. Razaviyayn, Z.-Q. Luo, and C. He, "An iteratively weighted MMSE approach to distributed sum-utility maximization for a MIMO interfering broadcast channel," *IEEE Trans. Signal Process.*, vol. 59, no. 9, pp. 4331–4340, Sep. 2011.